Impacts of negative to positive capacities ratios on the performance of next-generation lithium-ion batteries

Ge Mu [a,b], *Shubham Agrawal* [a], *Poom Sittisomwong* [a], *Peng Bai* [a,c,*]

[a] Department of Energy, Environmental & Chemical Engineering, Washington University in St. Louis, St. Louis, Missouri 63130, United States

[b] School of Materials Science and Engineering, Beijing Institute of Technology, Beijing Key Laboratory of Environment Science and Engineering, Beijing 100081, China

[c] Institute of Materials Science and Engineering, Washington University in St. Louis, St. Louis, Missouri 63130, United States

* Email: pbai@wustl.edu

Abstract:

The capacity ratio between the negative and positive electrodes (N/P ratio) is a simple but important factor in designing high-performance and safe lithium-ion batteries. However, existing research on N/P ratios focuses mainly on the experimental phenomena of various N/P ratios. Detailed theoretical analysis and physical explanations are yet to be investigated. Here, by combining physics-based modeling and experiments, quantitative understandings of the effects of different N/P ratios for batteries with the silicon-graphite composite anode and the $LiNi_{0.8}Co_{0.1}Mn_{0.1}O_2$ cathode (Si-Gr/NMC811) are investigated. The results reveal that higher N/P ratios enabled better cycling performance, while the choice of the ratio is a multi-facet optimization problem. Both the equilibrium open-circuit potential and the dynamic overpotentials of various electrochemical polarization are found to affect the electrode utilization at different N/P ratios. Due to the opposite trends of electrode utilization with respect to the N/P ratio, batteries need to be optimized with the help of mathematical simulations to identify the best design, rather than using a simple N/P ratio of 1, to meet specific needs.

Keywords:

N/P ratios, Si-Gr/NMC811 full cells, electrode utilization, overpotentials

1. Introduction

Lithium-ion batteries (LIBs) are widely used in portable electronic products[1,2], electric vehicles, and even large-scale grid energy storage[3,4]. While achieving higher energy densities is a constant goal for battery technologies, how to optimize the battery materials, cell configurations and management strategies to fulfill versatile performance requirements is equally important and challenging[5,6].

As one of the most promising designs, pairing a silicon-graphite (Si-Gr) composite anode with a Nickel-rich layered oxide cathode has become a successful commercial technology that can provide a cell-level energy density of > 300 Wh kg^{-1}. Recently, Son et al combined a Si-Gr anode with lithium nickel-manganese-cobalt oxide cathode, achieving a high specific energy of 333 Wh kg^{-1} with stable cycling[7]. Karuppiah et al fabricated Si nanowires-grown-on-graphite composite as anode and paired it with Nickel-rich layered oxide cathode to obtain full cells that can display a high energy density of 414 Wh kg^{-1} with a capacity retention of 70% over 300 cycles[8]. Jia et al constructed a full cell with Si-based material as anode and lithium nickel-manganese-cobalt oxide as cathode, demonstrating > 92% capacity retention over 500 cycles[9].

Despite the impressive performance, balancing the anode and the cathode, characterized by the capacity ratio between the negative and the positive electrode (N/P ratio), is still a much-needed but multi-faceted challenge, for which the fundamental understandings and optimization strategies remain to be investigated in a rigorous manner[10,11]. The N/P ratio is critical for battery safety and performance[12–14].

To avoid lithium plating during the charging process that may lead to fires or explosions[12,15], an N/P ratio > 1 is commonly adopted in the full cell design[16]. But surprisingly there is a study showing that an N/P ratio of 0.80 in Si-C/$LiFePO_4$ full cell does not lead to lithium plating, demonstrating a long and stable cycle life[10]. The N/P ratio is also a critical design parameter that can influence the utilization level of the electrodes, affecting the overall performance and cell-level energy density. For example, the Gr/$LiFePO_4$ full cells with a low N/P ratio of 0.87 could gain the highest cell-level specific capacity at the initial stage of cycling, but suffered from faster cell degradation[14]. The SiO_x-Gr/$LiNi_{0.8}Co_{0.15}Al_{0.05}O_2$ pouch cells developed by Chen et al achieved the best cycling stability at an N/P ratio around 1.03, preserving 80.2% of its capacity after 500 cycles[13]. In the case of lithium metal battery[15], N/P ratios are still an important design criterion. It has been demonstrated that for lithium metal cells with N/P ratios > 2.5, initial cycles were very stable, but usually followed by a sudden capacity drop[15]. An optimal N/P ratio of 1 has been identified,[15] as it balances well the rates of Li consumption, electrolyte depletion, and solid–electrolyte interphase formation, thus decelerating the increase of cell polarization and extending cycle life, resulting in long cycle life of 600 cycles with a capacity retention of 76%.

Investigating the effects of N/P ratios usually requires exhaustive experiments, which are apparently time-consuming. Predictive mathematical simulations[17] become a useful tool to complement such experimental studies, providing fundamental physical explanations for the observed experimental phenomena[18,19].

Here, we adopt the multiphase porous electrode theory (MPET) and use the

open-source code[20–22] to develop a model for Si-Gr/NMC811 batteries. The model was validated and calibrated with parameters and performance data from both the commercial cells reported in the literature and coin cells made in our lab. The combined theoretical and experimental study allows us to obtain physics-based explanations and quantitative understandings of the effects of different N/P ratios.

2. Methods

2.1 Mathematical model

The schematic of the Si-Gr/NMC811 LIBs is displayed in Figure 1. Each of the Si-Gr anode, the separator, and the NMC811 cathode domains was discretized into twenty volumes along the x-axis. Each volume contains two representative particles. This full cell model based on the MPET python package[20–22] is comprised of three modules: (i) Si-Gr anode, (ii) NMC811 cathode, and (iii) system. Both electrode modules can be called from the system module, thus coupling the dynamic processes in the active materials with those in the electrolyte. The MPET model captures four processes: (1) The *electron conduction* in the Si-Gr anode, NMC811 cathode, and the current collectors governed by Ohm's law; (2) The *ion diffusion* in the electrode active particles controlled by Fick's laws of diffusion; (3) The *charge transfer reaction* kinetics at the electrode-electrolyte interface determined by the modified Butler-Volmer equation; (4) The *ion transport* in the electrolyte based on the concentrated electrolyte theory[23]. The kinetic model for the solid-solution material is a simplified version of ion intercalation and phase transformation dynamics modeled by the Cahn-Hilliard-Reaction kinetics[20,24]. This physics-based model enables predictions

of the internal dynamics within the battery, such as liquid-phase Li^+ concentration, solid-phase Li^+ concentration, reaction rates, solid-phase potential, electrolyte phase potential, and overpotentials[20–22].

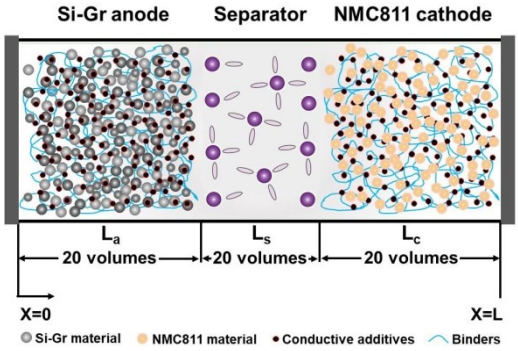

Figure 1. Schematic of the Si-Gr/NMC811 system with the one-dimensional mathematical domains defined in the MPET model.

The system is constrained by the following boundary conditions. The fluxes, concentrations, and potentials are treated as continuous between the separator and the electrode. Since the electrons do not come into the electrolyte, the electrode/separator interface is considered electrically insulated.

Battery parameters were extracted from the study of a commercial Si-C/NMC811 (INR18650-MJ1, LG Chem) battery[25]. The mass ratio of Si : Gr : inactive material (binder and conductive additives) was set to 3.5 : 87.5 : 9. This composition yields an estimated gravimetric capacity of the anode as 415 mAh g^{-1}, based on the theoretical specific capacities of natural Gr and nano-Si as 330 mAh g^{-1} and 3600 mAh g^{-1}, respectively[25–27]. The volumetric ratio of active material : inactive material : pores was calculated as 69.4 : 9 : 21.6, using the respective densities (2.24 g cm^{-3} for Si-Gr active material and 1.78 g cm^{-3} for inactive material) and the porosity of Si-Gr anode (21.6%)[25,28,29]. The total lithium site density within the Si-Gr anode was determined to

be 2.09×10^{28} Li m^{-3}.

A similar calculation was performed for the NMC811 cathode. The mass ratio of active: inactive material is 96: 4 while their volumetric ratio is 74.5: 8.4, considering the density of active material as 4.87 g cm^{-3} and the porosity of cathode[25,30] as 17.1%. The gravimetric capacity of the NMC811 cathode was set as 275.5 mAh g^{-1} and the total lithium site density within the NMC811 material[25,30] was calculated to be 3.01×10^{28} Li m^{-3}. The specific values of calibrated parameters for Si-Gr anode, NMC811 cathode, and separator are listed in Table 1.

Table 1. Parameters of Si-Gr/NMC811 full cell model.

Parameters	Si-Gr anode	Separator	NMC811 cathode
Shape	Sphere		Sphere
Density, g cm^{-3}	2.24		4.87
Particle radius, μm	6.1		3.8
Total Li site density within the solid, Li m^{-3}	2.09×10^{28}		3.01×10^{28}
Theoretical capacity, mAh g^{-1}	415		275.5
Solid diffusivity, m^2 s^{-1}	5×10^{-14}		5×10^{-13}
Transfer coefficient	0.5		0.5
Film resistance, Ω m^2	0.0035		0
Solid conductivity, S m^{-1}	100		0.17
Thickness, μm	86.7	12	66.2
Active material fraction	0.694		0.745

Porosity	0.216	0.45	0.171
Bruggeman coefficient	1.5	1.5	1.85

2.2 Experimental methods

The cathode slurry was prepared using the active material NMC811 (MTI Corporation), poly-vinylidene chloride binder (PVdF, >99.5%, MTI Corporation), and conductive acetylene black (35-40 nm, MTI Corporation) in the mass ratio of 96: 2: 2 with 1-methyl-2-pyrrolidinone (NMP) and coated on the aluminum foil. The resulting cathode was tested in the half cell to achieve a specific capacity of 170 mAh g^{-1}. The Si-Gr active material was prepared with Si: Gr as the mass ratio of 1: 25 by ball milling. The rotation speed is 400 rpm, ball size is 2mm, milling time is 6h when preparing Si-Gr. This active material was combined with the PVdF binder and conductive acetylene black in the mass ratio of 91: 4.5: 4.5 and dissolved in NMP to obtain the anode slurry. This anode slurry was cast with the doctor-blade method on separate copper foils with different gaps to alter the thickness, therefore achieving different final N/P ratios. The Si-Gr anodes were subjected to three formation cycles at 0.1 C rate in half cells with the electrolyte of 1M $LiPF_6$ in EC: DMC (50: 50 v/v) with 10% volume ratio of fluoroethylene carbonate (FEC) as additive. These precycled anodes were used along with fresh NMC811 cathodes in the Si-Gr/NMC811 full cells separated by a glass fiber separator in the electrolyte of 1M $LiPF_6$ in EC: DMC (50: 50 v/v) with 10% volume ratio of FEC. All the full cells with different N/P ratios were tested in galvanostatic conditions of 0.75 and 2.8 mA cm^{-2} based on the electrode diameters (Φ6 mm), between the cut-off voltages of 2.5 – 4.2 V,

for 100 cycles.

3. Results and Discussion

The original MPET theory has been validated in several different battery systems. The validation results of our customized MPET model can be found in the supplementary material and only briefly described here. We will focus primarily on the effects of different N/P ratios, their root causes, and practical implications.

3.1 Model validation

The mathematical model was first calibrated by the voltage profiles of Si-Gr/NMC811 full cell obtained through experiments[31] at various C rates from C/25 to 1C, as shown in Figure S1. The simulation results exhibit a good agreement with the experiment at both low or high C rates, confirming the validity of the parameters shown in Table 1. The model was adjusted into a half-cell configuration and further verified by the experimental half-cell data[31] from 0.025C to 0.5C, as shown in Figures S1c and S1d. The voltage profiles of Si-Gr/NMC811 full cells obtained from our own cells with different N/P ratios are compared with the simulation results. As presented in Figure S2, the consistency of simulation results and experimental results further proves the accuracy of the model.

3.2 Effect of N/P ratios on Si-Gr/NMC811 full cell performance

Si-Gr/NMC811 full cells with various N/P ratios were obtained by varying the anode thickness while keeping the cathode thickness fixed. This method ensures an accurate estimation of the full capacity of the cathode from its specific capacity. The

Si-Gr anodes, however, were precycled 3 times at 0.1 C rate in the respective half cells to enable complete and uniform SEI formation. The full capacity of the anode, is also obtained from the formation cycles using the capacity of the 2nd discharge (lithiation) in half cells. The resultant N/P ratios varying from 0.31 – 2.24 were obtained, allowing detailed analysis on N/P ratios in a wide range that complements existing studies[10–14].

It is noteworthy that the absolute value of current will change with the variety of electrode thickness even under the same C rate. Hence, the full cell is investigated under the same actual current density, not the same C rate, for fair and consistent comparisons. As the N/P ratio increases, the *total capacity* of the full cell also increases as reflected by both the experimental and the simulation results (Figure 2a and c), which could be due to the thicker electrode thickness[12]. However, a decreasing gravimetric energy density of full cell was observed in both experimental and simulation cases (Figure 2b and d), which are consistent with the references[10,11,14,17]. The similar values of capacity from experiment and simulation further demonstrate that our Si-Gr/NMC811 full cell model is accurate and predictive, which could facilitate the full cell design. It is not surprising then, the state of charge (SOC) of the Si-Gr/NMC811 full cell at the cut-off voltage will also be influenced by the N/P ratio. As shown in Figures 2e and f, the cut-off SOC decreases with the increase in N/P ratio in the N/P < 1 regime. In contrast, in the N/P > 1 regime, the SOC increases with increasing N/P ratio. Note that at low N/P ratios, the SOCs in the first few cycles could be higher than 100% due to additional but unwanted lithium plating. See further

tests and discussions below.

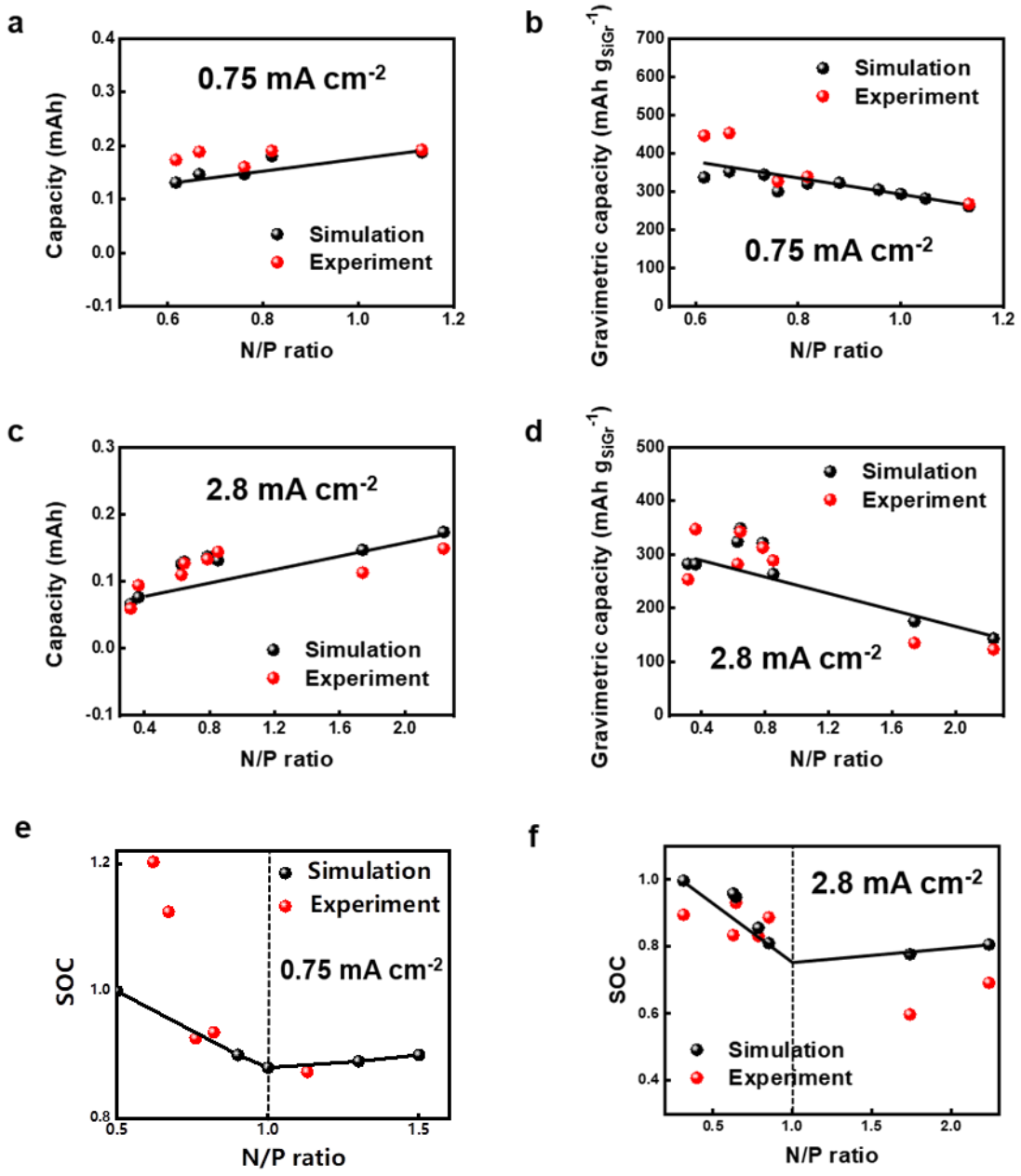

Figure 2. The effect of N/P ratios on the performance of Si-Gr/NMC811 full cell. The total capacity of Si-Gr/NMC811 full cell under the same current density of (a) 0.75 mA cm^{-2} and (c) 2.8 mA cm^{-2}, the gravimetric capacity of Si-Gr/NMC811 full cell based on the mass of Si-Gr anode under the same current density of (b) 0.75 mA cm^{-2} and (d) 2.8 mA cm^{-2}, the SOC of Si-Gr/NMC811 full cell under the same current density of (e) 0.75 mA cm^{-2} and (f) 2.8 mA cm^{-2}.

While lowering the external current density is in general a viable option to improve the electrode utilization due to reduced reaction overpotential, it can increase the chances of lithium metal plating on the Si-Gr anodes before reaching the cut-off voltage, especially in cells with lower N/P ratios. To test this hypothesis, we conducted experiments at an N/P ratio of 0.36 at the current density of 0.75 mA cm^{-2} and observed the "over-utilization" of Si-Gr anode (due to Li plating) reaching beyond 100% (obtained from the corresponding C rate) in the 2^{nd} charge (lithiation of Si-Gr), as shown in Figure S3. In addition, the Coulombic efficiency in the 2^{nd} cycle remained ~60%, suggesting a high loss of capacity, unlike at the higher current density of 2.8 mA cm^{-2} where the Coulombic efficiency is more than 95% from the 2^{nd} cycle onwards. It took 25 cycles for the Coulombic efficiency to go above 90% at a low N/P ratio = 0.36, but led to a very low capacity retention of 7% after 100 cycles.

Figure 3a displays the experimental capacity retention of Si-Gr/NMC811 full cell under a current density of 2.8 mA cm^{-2}. After 100 cycles, the cell with a higher N/P ratio exhibits improved capacity retention (Figure 3a and b), which suggests that increasing the N/P ratio of Si-Gr/NMC811 full cell could be beneficial for cycling performance. As the N/P ratio is increased, the number of cycles to reach 90% Coulombic efficiency reduces at 0.75 mA cm^{-2} (Figure 3c). The challenge of Li plating in addition to the other degradation factors significantly affects the capacity retention at lower current density in comparison to that at high current density, as shown in Figure 3d. Thus, lower current densities can result in high electrode utilization initially, but at a cost of possible lithium metal plating that raises a

potential safety concern.

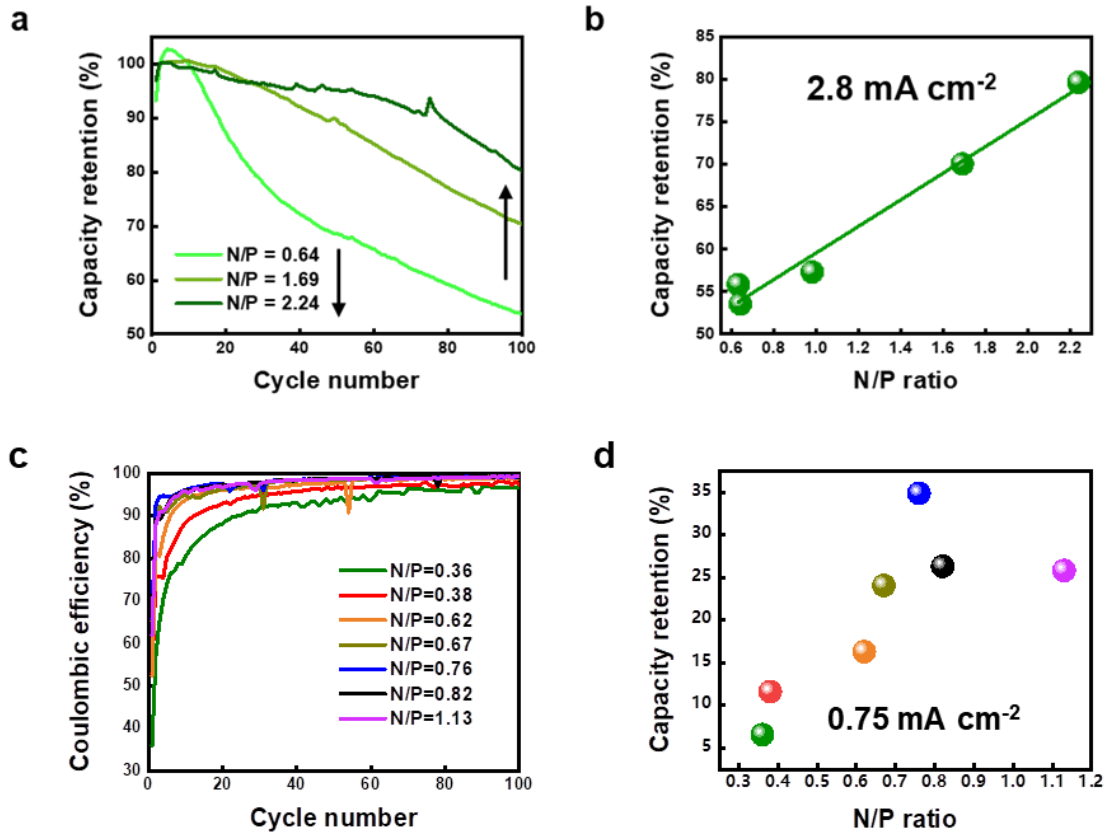

Figure 3. The effect of N/P ratios on the cycling performance of Si-Gr/NMC811 full cell. (a) Capacity retention vs. cycle number of Si-Gr/NMC811 full cell under the current density of 2.8 mA cm^{-2} with various N/P ratios. (b) The effect of N/P ratios on the capacity retention after 100 cycles of Si-Gr/NMC811 full cell under the current density of 2.8 mA cm^{-2}. (c) Coulombic efficiency vs. cycle number of Si-Gr/NMC811 full cell under the current density of 0.75 mA cm^{-2} with various N/P ratios. (d) The effect of N/P ratios on the capacity retention after 100 cycles of Si-Gr/NMC811 full cell under the current density of 0.75 mA cm^{-2}.

3.3 Electrode utilization

The above observations related to SOC may be attributed to electrode utilization. We performed full cell experiments and determined the utilization level by using the

2^{nd} charge capacity. In the simulation, the electrode utilization level can be estimated by the extent of delithiation and lithiation in the cathode and anode, respectively, during the charging process. The comparisons between experiments and simulations are displayed in Figure 4. As N/P ratios increase, the anode utilization decreases, while the cathode utilization increases under a current density of 2.8 mA cm^{-2}, as presented in Figures 4a and b. Likewise, the cathode can be utilized more while the anode is utilized lesser on increasing the N/P ratio under 5.48 mA cm^{-2} current density, as exhibited in Figure 4c. A lower N/P ratio leads to a lower level of cathode utilization but a higher level of anode utilization. In N/P < 1 regime, the maximum capacity provided by the anode is less than the maximum capacity of the cathode. Therefore, the anode would only accommodate fewer lithium ions and become quickly fully lithiated, exhibiting a high utilization. However, the anode's demand for fewer lithium ions reduces the degree of delithiation in the cathode, resulting in low utilization of the cathode.

The higher level of anode utilization when N/P < 1 apparently would result in a higher maximum SOC, as revealed in the anode utilization (yellow line) on the N/P < 1 side in Figure 4d. As the N/P ratio increases in the N/P > 1 regime, the cathode utilization also increases, resulting in the increase in the maximum global SOC, as exhibited in the cathode utilization (red line) on the N/P > 1 side in Figure 4d. Therefore, the global SOC is governed by the anode utilization in the N/P < 1 regime, or by the cathode utilization in the N/P > 1 regime, as depicted in Figure S4.

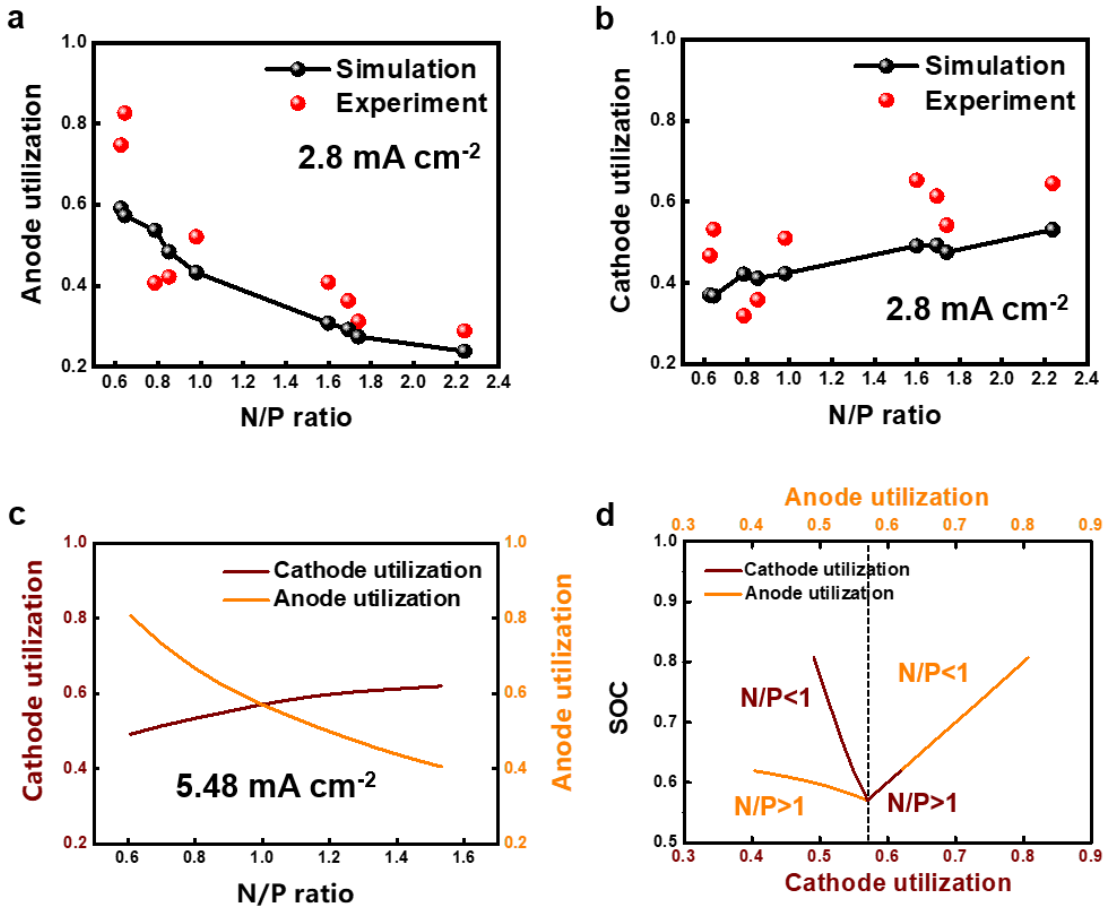

Figure 4. The effect of N/P ratios on electrode utilization. (a) The anode utilization under the current density of 2.8 mA cm^{-2}, (b) cathode utilization under the current density of 2.8 mA cm^{-2}, (c) electrode utilization under the current density of 5.48 mA cm^{-2}. (d) The relationship between electrode utilization and the SOC.

For Si-based anode, volume expansion during lithiation is a significant challenge for stable cycling. If the total capacity of Si anode material is utilized, i.e. the complete lithiation of Si, the large volume expansion would cause irreversible damage of the Si-Gr composite anode very quickly. By adjusting the N/P ratio to higher values, the resultant lower utilization of Si-Gr anode will enable improved capacity retention of Si-Gr/NMC811 full cell, as presented in Figure 3a and 3b.

3.4 Electrochemical dynamic through the porous structures

As revealed in the above section, the global SOC of the full cell is governed by the utilization of the limiting electrode and the global SOC varies non-monotonically with the N/P ratios. While the observation is surprising, it is necessary to investigate their fundamental cause for a better understanding. We compared three cases N/P = 0.8, 1.0, and 1.35, for a careful inspection of the underlying mechanism. Figure 5a reveals that the full cell with N/P = 1.0 reached the cut-off voltage earlier than the other two cases under the same kinetic conditions, resulting in the lowest SOC. Intuitively, the lowest global SOC at N/P = 1.0 would appear to be a result of a higher net overpotential compared to the other cases, and similarly, N/P = 0.8 should have the lowest net overpotential. However, Figure 5a indicates that N/P = 0.8 cell experienced the largest net overpotential, followed by N/P = 1.0 and N/P = 1.35 cells. The net overpotential can be broken down into the reaction overpotential, the Ohmic drop, and the concentration overpotential.

The reaction overpotential is from the reaction kinetics governed by the modified Butler-Volmer equation, while the Ohmic drop depends on the absolute current and the internal resistance. According to the modified B-V equation, the observed current density depends on the concentration-dependent exchange current density and the reaction overpotential. During battery charging, the net reaction overpotential is a contribution from both the lithiation reaction at anode and the delithiation reaction at the cathode. Since the applied current density and the exchange current density were consistent among all three cases, the net reaction overpotential remained unaffected

by the different N/P ratios as shown in Figure 5b. However, Figure 5c shows that the Ohmic drop would differ among the three cases, since the actual C-rates depend on the N/P ratio. Moreover, the Ohmic drop followed the same behavior as the net overpotential shown in Figure 5a. It should be noted that since the variations in the electrolyte concentration are very similar with negligible gradients in all three cases (Figure S5), their concentration overpotentials are also comparable.

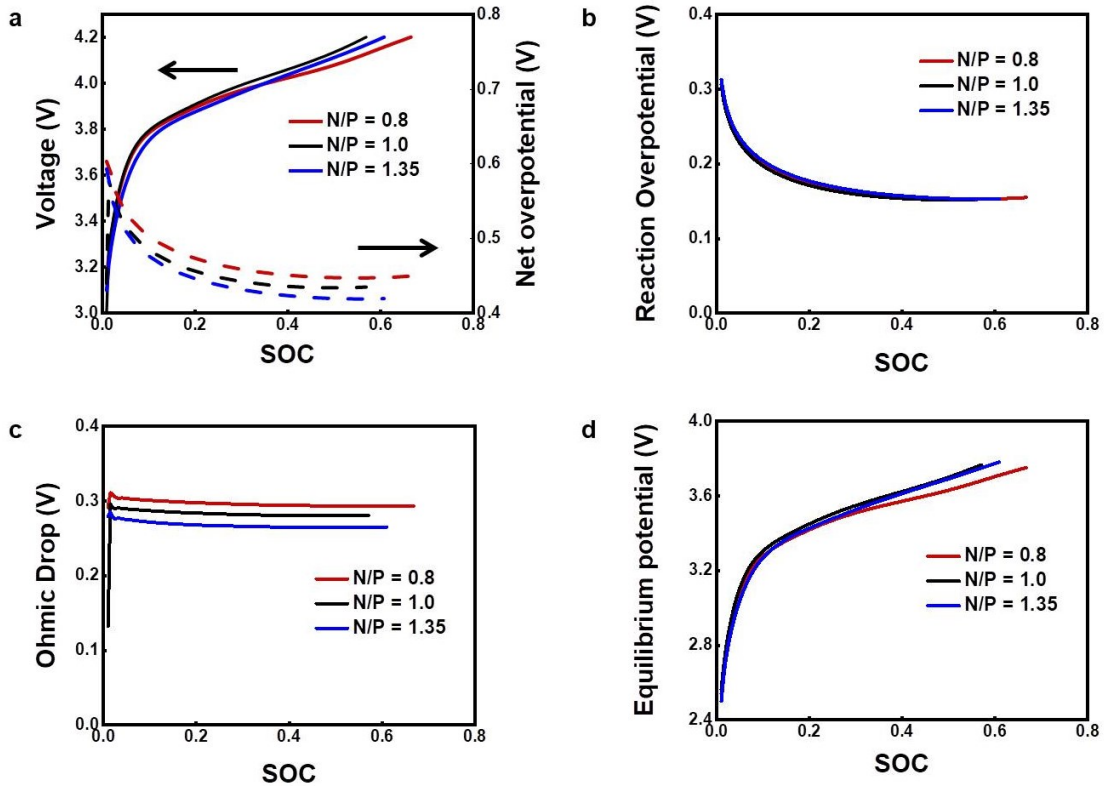

Figure 5. Thermodynamic and dynamic reasons of cell-level SOCs at various N/P ratios. (a) The voltage and net overpotential, (b) net reaction overpotential calculated from B-V kinetics, (c) effective Ohmic drop as the difference between the net overpotential and the net reaction overpotential, and (d) equilibrium potentials with respect to SOC.

The above revelation enabled us to evaluate the observed trend of the net overpotential, the underlying reason behind the lowest global SOC at N/P = 1.0 still

needs investigation. Upon careful inspection, it can be seen in Figure 5d that the variation of the equilibrium potential with global SOC differs among the three cases. The equilibrium potential at N/P = 0.8 has the lowest slope compared to the other two cases and its combination with a high net overpotential would still result in the lowest slope in the overall voltage profile, resulting in the highest global SOC at the cut-off voltage. The above observation confirms the sensitive dependence on the equilibrium voltage curve. Since the equilibrium voltage profile remains unchanged for a fixed N/P ratio, tuning the cell internal resistance will impact the Ohmic drop within the cell, thus achieving a higher global SOC at high current densities.

4. Conclusions

In this work, we have combined experiments and simulations to investigate the performance of Si-Gr/NMC811 batteries at various N/P ratios from 0.31 to 2.24. The results showed that the seemingly simple N/P ratio embodies a multi-facet optimization problem, requiring quantitative understandings of equilibrium properties of the battery materials and dynamic polarizations within the whole system. For the Si-Gr/NMC811 full cells investigated here, increasing the N/P ratio is in favor of achieving better cycling life, but electrode utilization levels in the anode and cathode show opposite trends. For other batteries employing different materials and configurations, our experimentally verified mathematical model based on the multiphase porous electrode theory (MPET), in which the material properties and battery configurations can be easily adjusted, offers a convenient tool to test out the

specific impacts of the N/P ratios for the selected systems. Optimizing the N/P ratio, in addition to the material and structural design, can facilitate the customization of battery performance to meet different needs.

Acknowledgment

P.B. acknowledges the faculty startup support from Washington University in St. Louis. The electrochemical experiments and simulations of anodes were partially supported by a National Science Foundation grant (Award No. 2044932). The materials characterization experiments were partially supported by IMSE (Institute of Materials Science and Engineering) and by a grant from InCEES (International Center for Energy, Environment and Sustainability) at Washington University in Saint Louis.

References

1. Tarascon, J. M. & Armand, M. Issues and challenges facing rechargeable lithium batteries. *Nature* **414**, 359–367 (2001).
2. Armand, M. & Tarascon, J.-M. Building better batteries. *Nature* **451**, 652–657 (2008).
3. Das, U. K. *et al.* Advancement of lithium-ion battery cells voltage equalization techniques: A review. *Renew. Sustain. Energy Rev.* **134**, 110227 (2020).
4. Zubi, G., Dufo-López, R., Carvalho, M. & Pasaoglu, G. The lithium-ion battery: State of the art and future perspectives. *Renew. Sustain. Energy Rev.* **89**, 292–308 (2018).
5. Zilberman, I., Sturm, J. & Jossen, A. Reversible self-discharge and calendar aging of 18650 nickel-rich, silicon-graphite lithium-ion cells. *J. Power Sources* **425**, 217–226 (2019).
6. Li, H., Liu, C., Kong, X., Cheng, J. & Zhao, J. Prediction of the heavy charging current effect on nickel-rich/silicon-graphite power batteries based on adiabatic rate calorimetry measurement. *J. Power Sources* **438**, 226971 (2019).
7. Son, Y. *et al.* Calendering-Compatible Macroporous Architecture for Silicon–Graphite Composite toward High-Energy Lithium-Ion Batteries. *Adv. Mater.* **32**, 1–8 (2020).
8. Karuppiah, S. *et al.* A Scalable Silicon Nanowires-Grown-On-Graphite Composite for High-Energy Lithium Batteries. *ACS Nano* **14**, 12006–12015 (2020).

9. Jia, H. *et al.* Hierarchical porous silicon structures with extraordinary mechanical strength as high-performance lithium-ion battery anodes. *Nat. Commun.* **11**, 1–9 (2020).

10. Song, B. F., Dhanabalan, A. & Biswal, S. L. Evaluating the capacity ratio and prelithiation strategies for extending cyclability in porous silicon composite anodes and lithium iron phosphate cathodes for high capacity lithium-ion batteries. *J. Energy Storage* **28**, 101268 (2020).

11. Baasner, A. *et al.* The Role of Balancing Nanostructured Silicon Anodes and NMC Cathodes in Lithium-Ion Full-Cells with High Volumetric Energy Density. *J. Electrochem. Soc.* **167**, 020516 (2020).

12. Kim, C. S., Jeong, K. M., Kim, K. & Yi, C. W. Effects of Capacity Ratios between Anode and Cathode on Electrochemical Properties for Lithium Polymer Batteries. *Electrochim. Acta* **155**, 431–436 (2015).

13. Chen, Z. *et al.* Effect of N/P ratios on the performance of LiNi0.8Co0.15Al0.05O2||SiOx/Graphite lithium-ion batteries. *J. Power Sources* **439**, 227056 (2019).

14. Abe, Y. & Kumagai, S. Effect of negative/positive capacity ratio on the rate and cycling performances of LiFePO4/graphite lithium-ion batteries. *J. Energy Storage* **19**, 96–102 (2018).

15. Niu, C. *et al.* Balancing interfacial reactions to achieve long cycle life in high-energy lithium metal batteries. *Nat. Energy* doi:10.1038/s41560-021-00852-3.

16. Kasnatscheew, J. *et al.* A Tutorial into Practical Capacity and Mass Balancing of Lithium Ion Batteries. *J. Electrochem. Soc.* **164**, A2479 (2017).

17. Doyle, M., Fuller, T. F. & Newman, J. Modeling of Galvanostatic Charge and Discharge of the Lithium/Polymer/Insertion Cell. *J. Electrochem. Soc.* **140**, 1526 (1993).

18. Doyle, M., Fuller, T. F. & Newman, J. The importance of the lithium ion transference number in lithium/polymer cells. *Electrochim. Acta* **39**, 2073–2081 (1994).

19. Fuller, T. F., Doyle, M. & Newman, J. Simulation and Optimization of the Dual Lithium Ion Insertion Cell. *J. Electrochem. Soc.* **141**, 1 (1994).

20. Bazant, M. Z. Theory of Chemical Kinetics and Charge Transfer based on Nonequilibrium Thermodynamics. *Acc. Chem. Res.* **46**, 1144–1160 (2013).

21. Ferguson, T. R. & Bazant, M. Z. Nonequilibrium Thermodynamics of Porous Electrodes. *J. Electrochem. Soc.* **159**, A1967 (2012).

22. Smith, R. B. & Bazant, M. Z. Multiphase Porous Electrode Theory. *J. Electrochem. Soc.* **164**, E3291 (2017).

23. Dargaville, S. & Farrell, T. W. A comparison of mathematical models for phase-change in high-rate LiFePO4 cathodes. *Electrochim. Acta* **111**, 474–490 (2013).

24. Robert, W. *et al.* Kinetics of Materials. *Wiley* (2005).

25. Sturm, J. *et al.* Modeling and simulation of inhomogeneities in a 18650 nickel-rich, silicon-graphite lithium-ion cell during fast charging. *J. Power*

Sources **412**, 204–223 (2019).

26. Magasinski, A. *et al.* High-performance lithium-ion anodes using a hierarchical bottom-up approach. *Nat. Mater. 2010 94* **9**, 353–358 (2010).

27. Dash, R. & Pannala, S. RETRACTED ARTICLE: Theoretical Limits of Energy Density in Silicon-Carbon Composite Anode Based Lithium Ion Batteries. *Sci. Reports 2016 61* **6**, 1–7 (2016).

28. Long, C. M., Nascarella, M. A. & Valberg, P. A. Carbon black vs. black carbon and other airborne materials containing elemental carbon: Physical and chemical distinctions. *Environ. Pollut.* **181**, 271–286 (2013).

29. Liu, G. *et al.* Optimization of Acetylene Black Conductive Additive and Polyvinylidene Difluoride Composition for High Power Rechargeable Lithium-Ion Cells. *ECS Trans.* **6**, 45 (2007).

30. Jung, R., Metzger, M., Maglia, F., Stinner, C. & Gasteiger, H. A. Oxygen Release and Its Effect on the Cycling Stability of LiNixMnyCozO2 (NMC) Cathode Materials for Li-Ion Batteries. *J. Electrochem. Soc.* **164**, A1361 (2017).

31. Anseán, D. *et al.* Mechanistic investigation of silicon-graphite/LiNi0.8Mn0.1Co0.1O2 commercial cells for non-intrusive diagnosis and prognosis. *J. Power Sources* **459**, 227882 (2020).